Available online at www.sciencedirect.com

ScienceDirect

Polar Science 8 (2014) 24–39

http://ees.elsevier.com/polar/

An observational study of radiation temperature inversions in Fairbanks, Alaska

Julie Malingowski [a,b,c,1], David Atkinson [b,c,d], Javier Fochesatto [b], Jessica Cherry [c,e,*], Eric Stevens [a,f]

[a] *NOAA's National Weather Service, WFO Fairbanks, PO Box 757345, Fairbanks, AK 99775-7345, USA*
[b] *Department of Atmospheric Sciences, College of Natural Science and Mathematics, University of Alaska Fairbanks, 903 Koyukuk Drive, Fairbanks, AK 99775-7320, USA*
[c] *International Arctic Research Center, University of Alaska Fairbanks, PO Box 757340, Fairbanks, AK 99775-7340, USA*
[d] *University of Victoria, British Columbia, Canada*
[e] *Institute of Northern Engineering, University of Alaska Fairbanks, PO Box 755910, Fairbanks, AK 99775-5910, USA*
[f] *Geographic Information Network for Alaska, University of Alaska Fairbanks, 111B West Ridge Research Building, Fairbanks, AK 99775, USA*

Received 26 March 2013; revised 9 January 2014; accepted 15 January 2014
Available online 24 January 2014

Abstract

A series of high resolution radiosonde launches were conducted over seven case-study days spanning spring 2009 and fall/winter 2010 during clear and calm nights at Fairbanks, Alaska to evaluate the effects of solar radiation, snow covered surfaces and low-level winds on the formation and evolution of surface-based temperature inversions (SBI). Transition seasons were selected because strong nighttime radiation cooling allows well-defined inversions to form while sufficient daytime solar heating allows the observation of dissipation processes in the sub-arctic latitudes. During the fall/winter period, co-located Doppler phased array acoustic soundings (SODAR) were carried out. The height of the SBI retrieved by radiosonde and SODAR did not differ more than 50 m. However, the SODAR profiles display a much more complex structure in the atmospheric boundary layer. Observations during this experiment demonstrated that the formation of the SBI is initiated by a rapid cooling at the surface followed by a steady columnar cooling and subsequent growth of the SBI depth overnight.

Keywords: Temperature inversion; Radiation balance; Arctic meteorology

1. Introduction

1.1. The basics

Steep, surface-based inversions (SBI) are common in the valleys of interior Alaska due to the frequent occurrence of thermodynamically stable air masses in the lower levels during wintertime, which in turn are caused by the large negative net surface radiation

* Corresponding author. IARC-UAF, 930 Koyukuk Dr., Fairbanks, AK 99775-7335, USA. Tel: +1 9074745730.
E-mail address: jcherry@iarc.uaf.edu (J. Cherry).
[1] Present address: NOAA's National Weather Service, WFO Grand Junction, 2844 Aviators Way, Grand Junction, CO 81506, USA.

1873-9652/$ - see front matter
http://dx.doi.org/10.1016/j.polar.2014.01.002

balance that is often present in high-latitude regions. Winter in high-latitudes brings low-solar angle conditions such that, on many days, shortwave downwelling radiation never exceeds upwelling longwave radiation. This allows a persistent negative net radiation balance situation at the surface, resulting in a continuous temperature decrease, which is propagated up into the lowest levels of the atmospheric boundary layer (ABL) (Wendler and Jayaweera, 1972). If the prevailing synoptic conditions dictate weak pressure gradient forces (resulting in low wind) then the air density gradient becomes strong enough that the lower levels (below ~1000 m Mean Sea Level–MSL) become decoupled from the rest of the troposphere. Under these conditions with low winds and a negative surface radiation balance, a SBI will develop. The top height of the temperature inversion is often defined to be the point at which the temperature begins to decrease with height.

A major influential factor in the formation of the high latitude SBIs is the presence of negative net radiation at the surface (Bradley et al., 1992). Inversion top height typically reaches several hundred meters above ground level. The difference in temperature between the ground surface and the top height of the inversion can approach 30 °C over a distance of a few hundred meters. These strong temperature gradients within the inversion layer are common in the sub-arctic region (Bradley et al., 1992).

The temperature gradient and height of the SBI are a function of various factors, including low level clouds and their physical properties, local boundary layer moisture and the presence of IR absorbing gases (i.e. CO_2, CO, H_2O), surface and upper level winds, heat flux from snowpack (Wexler, 1936; Hogan and Ferrick, 1997), longwave radiation divergence, low solar angle (Wendler and Nicpon, 1974), and topography. Clouds and moisture play the most important role in the short term (hours to days) to alter the radiation budget of the atmosphere (Andre and Mahrt, 1981), by their capacity to affect shortwave and longwave radiation transfer (Kahl et al., 1992). During winter at high latitudes the net radiation reaches relatively large, negative values (~ -20 Wm^{-2}) and, with low level shortwave radiation available to reverse surface cooling, inversions become susceptible to winds that can weaken or destroy them. Strong winds operating at the synoptic scale can cause large-scale horizontal advection of warm, relatively moist air masses, which can dissipate the SBI by increasing longwave downwelling radiation. Winds at the mesoscale, such as weak jets which develop above a strong thermal gradient, even if relatively weak ($\sim$3 ms^{-1}), can cause downward mixing of warmer air situated aloft into the inversion layer (Stull, 1988). Meso- and regional-scale winds, when at the surface, can also aid formation of an SBI. Simulations performed using a one-dimensional nocturnal boundary layer model by Estournel and Guedalia (1985) suggest that, even in the presence of weak winds, a stable layer can continue to thicken during the night if the negative radiative cooling is strong enough, even in the presence of upward divergence of infrared radiation (Estournel and Guedalia, 1985).

Surface boundary layer evolution is controlled by various spatial and temporal scales of variability, a fact that has been recognized for many years – Cermak (1971) comments on the need to introduce surface vertical and spatial heterogeneity to more realistically account for lower-atmosphere evolution. Despite this, there remains a lack of understanding of SBI formation in particular at locations where thermal radiation divergence is strong and persistent, such as in northern regions. An important problem stemming from this is the resulting, consistent warm bias in forecasts of surface air temperature. This is one of the major challenges for computer models and weather forecasters in northern or inversion-prone regions. For example, computer forecasting models can be biased by +15 C or more at the surface when conditions favor the formation of a stratified SBI in interior Alaska (Morton, 2009). This is in part due to the factors listed above, but also due to the poor ability of weather models to accurately predict inversion conditions under quasi-laminar flows in the lower ABL at representative scale resolution (Molders and Kramm, 2010).

1.2. Previous research

Previous work on SBIs in Interior Alaska and the broader sub-arctic/arctic region has focused largely on the classification of inversion patterns. Tilley and Weatherby (2001) focused on modeling the inversion during the ideal clear and calm weather conditions, while Hartmann and Wendler (2005) discuss the direction of winds in Fairbanks which give a persistent (77% of the time annually) formation of the SBI. It was found that the mean height of wintertime inversions is 520 m, with an average 11 °C from top to bottom of the inversion layer over a pressure span of 65 hPa (Hartmann and Wendler, 2005). Other work has considered SBI decay – Pepin et al. (2009) found that the thermal radiation divergence is great enough that, once winter has set in, the only way an SBI can be broken is through a change in synoptic conditions.

These research efforts on sub-arctic inversions have utilized the only consistent and long-term historical observational dataset available for inversion studies: profiles of temperature, humidity, pressure, wind speed and wind direction obtained by radiosondes launched twice a day at standard times – 15:00 AST and 03:00 AST. (Note: 03:00 AST launches as seen in the standard NOAA radiosonde database for all upper air stations are actually launched at 02:00 AST, therefore in this paper, what is considered as the standard 03:00 AST launch is shown as 02:00 AST, the actual time of launch).

1.3. Surface-based temperature inversions in Fairbanks, AK

Fairbanks, Alaska, located at 64.84 °N, is situated at the north end of the broad Tanana River Valley and is surrounded on three sides (north, east and west) by hills of approximately 500–700 m meter elevation. When radiation and synoptic conditions are suitable that is – clear and calm – cold pools of air masses form within the valleys and on the north sides of mountains. Such is the frequency of these conditions that a SBI is present in Fairbanks approximately 64% of the time during the winter months in a recent evaluation from January 2000 to February 2009 (Mayfield and Fochesatto, 2013). When the SBI forms, airborne particulate matter from combustion processes is trapped. This results in a significant increase in pollution concentration in Fairbanks, often exceeding Environmental Protection Agency (EPA) standards. These particulate concentrations impose health risks to local residents. With a growing population and rising fuel prices driving an increasing use of poor-efficiency woodstoves and wood boilers in the Fairbanks region, air quality forecasts are becoming more important to the residents of the area.

Model surface temperature prediction at different elevations in the middle Tanana Valley demonstrate that, under conditions of clear skies and calm winds, valley locations will be substantially colder than the hills. This thermal contrast disconnects the flows in the ABL from the free troposphere. Fig. 1 shows a topographic map of the Fairbanks area, and Fig. 2 illustrates an example of this thermal pattern using an infrared (IR) satellite image for the same area indicated in Fig. 1. In this IR image the "cold bowl" of Fairbanks is strongly contrasted with the warmer hills surrounding the city. The low level cooling feature is also clearly evident in the Yukon Flats, northeast of Fairbanks. In such cases, local

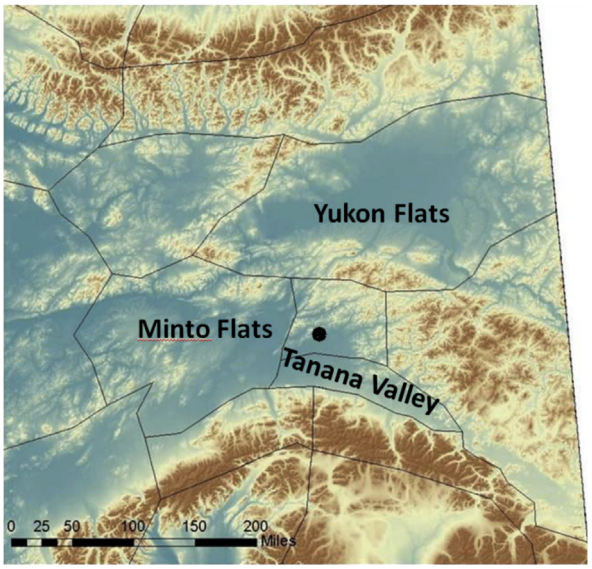

Fig. 1. Topography of the central Alaska Interior. Higher elevations are designated by brown and lower elevations are designated by green. Fairbanks is designated by the black dot. The lowland areas of the Tanana Valley (south of Fairbanks), Minto Flats (west of Fairbanks), and the Yukon Flats (northeast of Fairbanks) are visible (National Elevation Dataset for Alaska (USGS), National Weather Service Fairbanks).

topography, in the form of gravity-driven density flows, dominates the surface atmosphere when the pressure gradient force is weak, making accurate model representations of these thermodynamic features difficult. This in turn impacts the strength of the inversion forecasted by the US National Weather Service. This study's goal is to evaluate the effects of solar radiation, snow covered surfaces and low-level winds on the surface-based temperature inversion between the standard twice-daily launches provided by the US National Weather Service in Fairbanks, AK.

1.4. The surface-based temperature inversion and snowpack

During the spring/autumn seasons, a major shift in the pattern of high and low temperature occurs as the snowpack disappears/forms (Stevens, 2009). For this study, this time of year has been defined as the "transition season" to indicate the time of the year when the amount of radiation changes rapidly (i.e. the daylight increases or decreases a significant amount, by up to 7 min per day). For example, the day length increases from 13.5 h on April 1–17 h by April 30. The presence of a snowpack can modify the surface

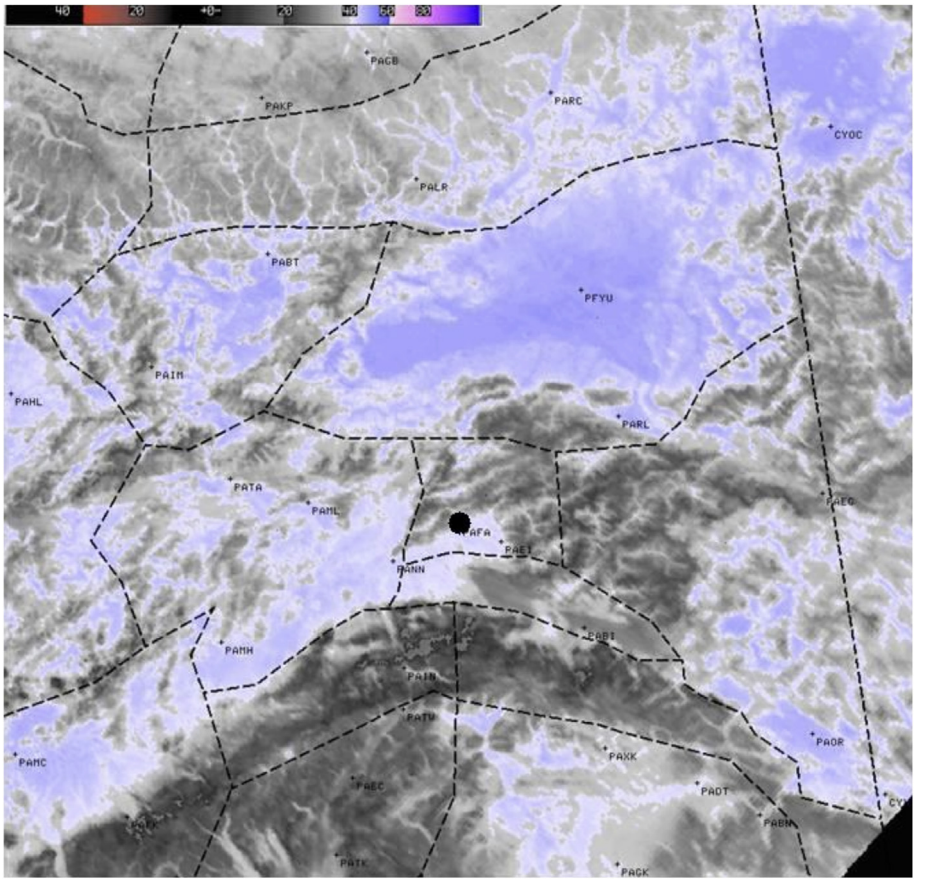

Fig. 2. Infrared satellite image of Fairbanks area during a clear night. Fairbanks is designated by the black dot. Gray designates areas of warmer temperatures and blue designates colder air (Polar Operational Environmental Satellite infrared image, February 2003, National Weather Service Fairbanks).

radiation balance through changes in conductive and latent heat fluxes, albedo, and surface emissivity (Walsh et al., 1985). The snowpack has a higher albedo than bare ground, therefore reflecting a greater proportion of incoming shortwave downward radiation. In these high-latitude cases, the main effect of snow on the strengthening of the SBI is that the presence of snow cover keeps the inversion from breaking during the daytime due to blockage of shortwave radiation absorption.

During the spring transition season the winter snowpack still exists in Fairbanks, but, despite its presence, rapidly increasing solar elevation and day length eventually combine to create daily incoming radiation totals large enough to cause large diurnal fluctuations. This positive energy balance breaks the inversion during the day, thus confining the SBI to the nighttime period after approximately March 15.

2. Methodologies

In order to capture details of the temporal evolution of the SBI formation, additional radiosonde launches were conducted in Fairbanks every two- to three-hours during a series of seven case-study periods. Study periods were chosen when specific, non-advective synoptic conditions, featuring clear skies and very low or nonexistent winds were present. Study period launches supplemented regular launches conducted at the 03:00 and 15:00 AST standard observing times. Launches were organized into seven detailed case studies for Fairbanks, Alaska. A single case study represents one afternoon-night-morning time cycle during which the additional radiosondes were launched from the NWS-NOAA station PAFA (70261) near Fairbanks International Airport. In addition, for some of the case studies, co-located acoustic sounding profiling was also

performed to determine the evolution of the ABL at 20 m vertical resolution and 15 min temporal profiling. Dates of case studies are displayed as one date for simplicity of reading. Each case study encompasses part of the day before; i.e. February 24th begins the evening of the 23rd (in AST) and continues through the night into the morning of the 24th.

Two broad time frames were chosen for this study – spring 2009, between the months of February and May, and fall 2009, between the months of September and November. January and February, the coldest part of the winter, were not selected because during this time, the only factor which will break the inversion in the sub-arctic region is a change in synoptic conditions or a small scale circulation (e.g., drainage flow) close to the mountain slopes. Case study dates were selected to examine the evolution of the formation of the SBI linked to night duration, and surface cover. Once the rational for the broader time frames was established, specific case study days were selected on fairly short notice when weather forecasts called for clear and calm conditions.

2.1. Instrumentation

Two different types of radiosonde systems were used in this study: the Vaisala RS-80, providing an average data resolution of 16 data points below 500 m, and the Sippican MKII GPS, providing an average data resolution of more than 100 data points below 500 m. The Vaisala radiosondes were used for the spring 2009 set of launches, and in summer 2009, the National Weather Service upgraded its equipment to the Sippican MKII GPS radiosonde, effective after September 2009. The Vaisala RS-80s vertical resolution translates into one datum every 6 s, or approximately every 30 m, depending on the balloon's rate of ascent. The Sippican MKIIs recorded vertical resolution translates into one datum several times per second, or approximately every 4–5 m. Although sampled at coarser vertical resolution, the February (Vaisala) soundings were still fully able to capture the main elements of the inversion lifecycle necessary for this study.

A Doppler acoustic sounder, Remtech PA-2 (hereafter called SODAR), was collocated with the radiosonde system at NWS-NOAA station PAFA (70261) for a period of time in the winter 2010–2011. The SODAR works at the central frequency of 2 kHz and consists of a monostatic antenna of 196 speakers mounted in a square section of ~ 1.7 m^2. The antenna is switched sequentially between emission and reception modes and background noise is measured and subtracted automatically. The acoustic backscattering is measured at 20 m resolution and 15 min integration periods, starting at 20 m above ground and continuing upward. The sound wave time-of-flight back to the antenna indicates the height at which the backscatter occurred. This intensity depends on the turbulent structure of the ABL and, due to the instrument's monostatic configuration, is only sensitive to the thermal structure of turbulence (C_T^2) depicting the ABL structure in great detail (Holmgren et al., 1975; Neff, 1975; Brown and Hall, 1978; Neff and Coulter, 1988; Coulter and Kallistratova, 2004). Following Beyrich and Weill (1993) the top height of the SBI layer can be calculated processing the SODAR backscatter profiles (C_T^2) by searching for the 50% decayed intensity of the backscatter pulse after the maximum of thermal turbulence intensity, for the cases where the inversion top height is above the 50 m minimum instrumental range.

2.2. Methodology for inversion retrieval

Seidel et al. (2010) reviewed and assessed the methodologies and uncertainties in retrieving the ABL heights at 505 stations dispersed at various, global locations, and used the top of the SBI as one way to indicate the height of the ABL. The presence of an identifiable SBI top is a reliable indicator of the occurrence of a stable atmospheric boundary layer (Seidel et al., 2010). The Seidel et al. methodology was used to identify the height of the top of the SBI, and define the thickness of the stable atmospheric boundary layer, however, the methodology was challenged by the sometimes non-trivial structures found within the SBI. Temperature profiles in the interior of Alaska can exhibit one or more complex slope changes, indicating the combined presence of stratified, isothermal, and inversion layers. The occurrence of multiple layers is especially prevalent near the land surface. These layers, when observed from the radiosonde profile, may present inversions typically classified as non-relevant because it is argued that they might be overridden by the eventual intra-day variation (Kahl, 1990; Serreze et al., 1992).

In this experiment, we demonstrate by means of this high-resolution radiosonde combined with Doppler SODAR measurements during the Winter Boundary Layer Experiment (Wi-BLEx) that these inversions and stratified levels are important and constantly present when favorable environmental conditions exist. Therefore, a numerical procedure was developed by Mayfield and Fochesatto (2013) to determine the

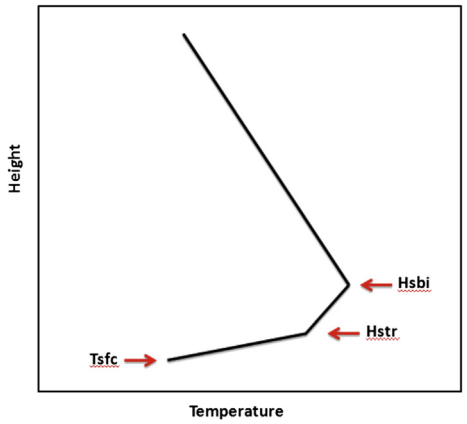

Fig. 3. Schema identifying the temperature at the surface (Tsfc), the top of the stratified layer (Hstr), and the top of the inversion layer (Hsbi).

heights and temperatures of the base and the top of stratified and inversion layers and those layers embedded in between (e.g., isothermals). With the purpose of identifying these layers, the temperature profile was assimilated into to a mathematical structure composed of a piecewise linear function established using an iterative numerical routine. The numerical routine minimizes the following error expression:

$$\varepsilon = \left\| T(z) - \sum_{k} m_k \cdot z + b_k \right\| \quad [1]$$

where $T(z)$ is the temperature profile, k is the number of layers retrieved, and the parameters m_k and b_k are function fitting. The convergence is controlled by the error fraction, calculated as the largest singular value of ε that reproduces inversions and stratified layers with an error difference of less than 1% and a gradient threshold larger than 0.1 °C/100 m. This numerical method does not introduce new points in the fitting process. It only uses the original points of the temperature profile and rather reduces the number of points according to the proposed error whenever the slope is below the gradient threshold. As a result, the temperature profile is now transformed into a data-structure containing the relevant thermodynamic characteristics of thermal layers found in the profile. The height of the top of an inversion layer is considered as the height where the temperature gradient changes from being positive upward to negative upward. The top of a stratified level is defined as the height where changes in the thermal gradient occurred preserving the positive sign (Fig. 3). The relevant atmospheric processes will be discussed in Section 4.1.

3. Results: timings and details of radiosonde launches

Of the seven case studies, four of them took place in spring and three in autumn (Table 1). Spring launch dates included one in late February, two in mid April

Table 1
Summary of the meteorological conditions during the Experiment at the National Weather Service, Fairbanks International Airport, Fairbanks, Alaska USA.

Date, time (UTC/AST) and # launches	Strongest surface wind during observation window	Ceiling development? (SCT or more)	Minimum temperature reached at PAFA (°C)	Snow depth (in)	Hours after sunset when min temp was reached	Hours before sunrise when min temp was reached	Max incoming radiation Wm^{-2}	Max solar angle
2/24/200916:00–10:00 AST7 launches	2.1 m/s (22:00–23:00 AST)	Y (BKN 10:00 AST)	−22	21	11	3	255	16
4/5/200919:00–09:00 AST7 launches	2.1 m/s (19:00–20:00, 03:00, 10:00 AST)	Y (BKN 19:00 AST)	−21	25	9	1	548	31
4/7/200919:00–09:00 AST7 launches	2.6 m/s (04:00 AST)	N	−16	25	10	0	568	32
5/1/200919:00–08:00 AST7 launches	2.1 m/s (20:00–21:00, 24:00–01:00 AST)	Y (BKN 19:00–20:00 AST)	3	0	7	2	750	41
10/13/200917:00–10:00 AST7 launches	2.1 m/s (24:00 AST)	N	−3	0	10	4	257	17
10/15/200917:00–10:00 AST7 launches	1.5 m/s (24:00, 7:00–08:00 AST)	N	−8	0	14	0	251	16
11/21/200917:00–11:00 AST 7 launches	1.5 m/s (17:00–18:00, 20:00–22:00 AST)	N	−36	7	13	5	23	5

and one in early May. The solar inclination angles during the spring experiment ranged from about 16° maximum solar angle (Feb.) to just over 40° (May). The maximum incoming solar radiation ranged from about 150 Wm^{-2} to nearly 700 Wm^{-2}, facilitating comparison of the surface-based temperature inversion at different points during the transition season. Autumn launches included two in mid-October and one in mid-November; maximum solar angle ranged from 5° (Nov.) to 17° (Oct.) and maximum incoming solar radiation ranged from 22 Wm^{-2} to 255 Wm^{-2}. Snow cover was present for 4 of the 7 case studies.

3.1. 24 February 2009 case summary

The temporal evolution of temperature on February 24th supports the hypothesis that the temperature inversion cools with height as the surface temperature reaches a minimum value. A notable cooling of the vertical profile with time maximizes just above the surface (near 75 m) between the 02:00 AST and 06:00 AST launches (Fig. 4), as winds remain calm (0–2 m/s).

The 24 February case study also provided insight into the influence of winds and their ability to alter the thermal structure in lower layers. A wind episode within the first 1000 m of the profiles produced a discernible effect on the vertical temperature structure. A short-duration event was apparent on the 19:00 AST launch, as indicated by a pronounced wind speed maxima at the height range from 150 to ~750 m AGL (Fig. 4). Although of short duration, the 22:00 AST profile shows a warming layer from about 50 m AGL to 225 m AGL and a very thin layer of cooling below, likely due to the wind speed maxima. The mechanism occurring with this warming layer can be attributed to the formation of a local-scale jet and subsequent downward mixing of warm air, as discussed in the Introduction.

3.2. 5 April 2009 case summary

During 5 April case study, a wind speed maximum is apparent around 500 m AGL, which shows an increase in speed over the period spanned by the 5:00 and 7:00 AST launches (Fig. 5). The surface temperature dropped 6 °C in 2 h after 23:00 AST. This is one of the largest 2-h drops observed in the experiment. As seen in the previous case on the 24 February, the lowest surface air temperature occurred between 5:00 and 7:00 AST right above the surface. The surface temperature never did cease to decrease, but continued

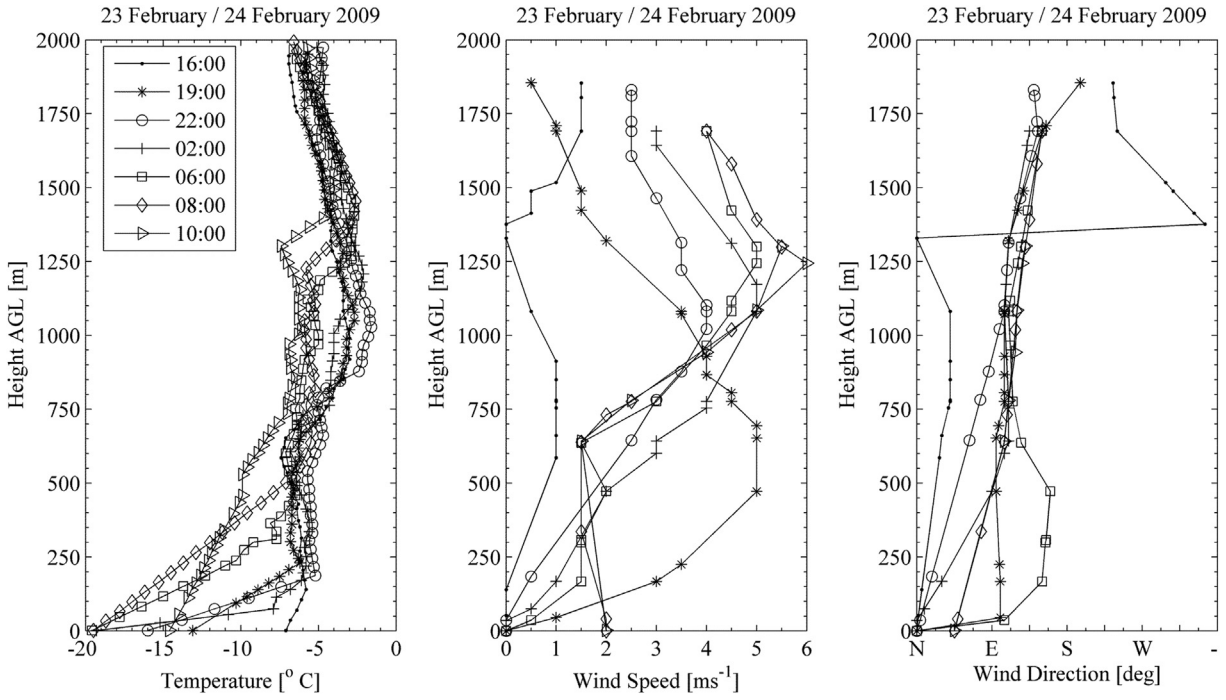

Fig. 4. Vertical structure of the SBI development post-sunset February 24, 2009. Sunset – 0250 UTC. The surface temperature decreases with time until a minimum temperature is reached. The atmosphere cools vertically after as is seen in the 1530 and 17 UTC data.

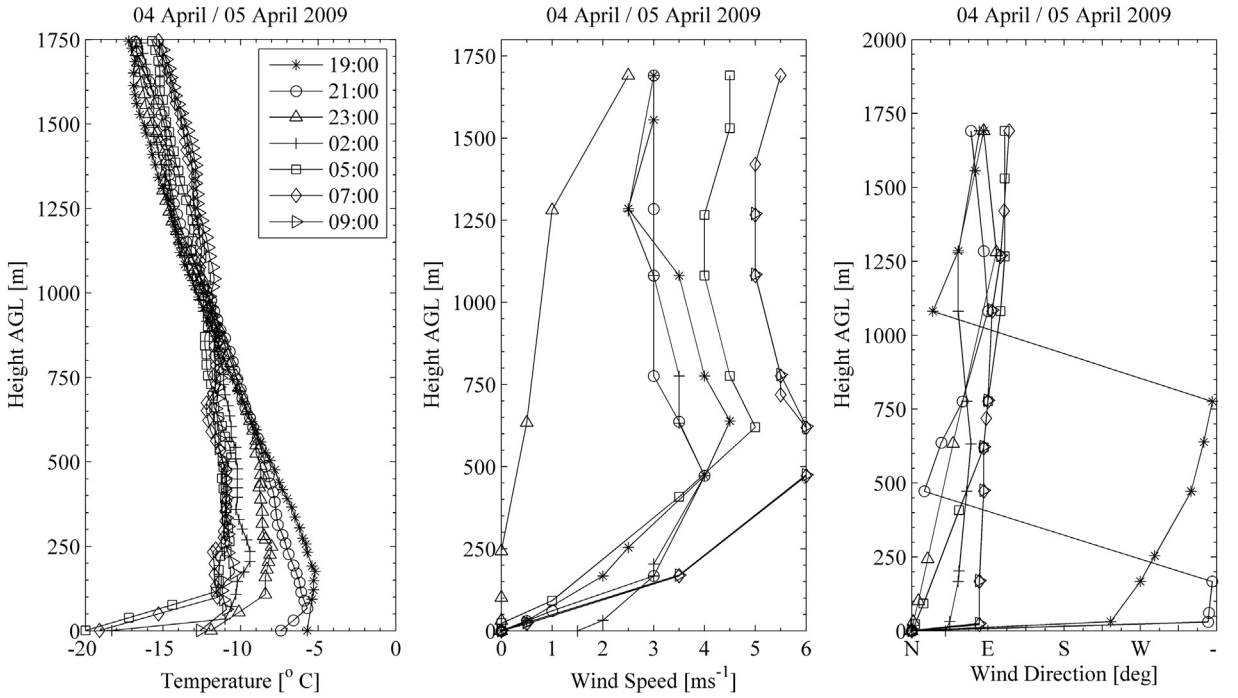

Fig. 5. Vertical structure of the SBI development post-sunset on April 5, 2009. Sunset – 19:55 AST.

until incoming solar radiation the next morning heated up the surface.

3.3. 7 April 2009 case summary

During the 7 April case study, the surface temperature decreased rapidly immediately after sunset, and once the surface temperature cooled, the inversion layer began to deepen with height as the longwave upwelling radiation cooling proceeded (Fig. 6).

The profile reached its coldest surface temperature of the evening during the 7:00 AST launch. The three launches near or after sunset at 20:01 AST verified very similar vertical profiles above the inversion top height. Winds above the surface level were nearly nonexistent on 7 April. On 7 April, the temperature profile above 600 m AGL remains consistent over the entire series of radiosonde launches, likely due to the low wind speed (Fig. 7). A cooling process above the surface occurs between the 5:00 and 7:00 AST launches. The influence of a short period of increased wind was noted at the 2:00 and 5:00 AST launches, both of which exhibited large temperature drops in the 0–400 m AGL elevation region coincident with the zone of wind speed maxima observed at these times. The processes observed make the case for higher frequency of launches, because of the important thermal structures that develop at the time of formation and breakup of the SBI.

During this set of balloon launches it should be noted that there are similarities and differences to the 5 April launches, which have an almost identical amount of incoming solar radiation, being only two days apart. Similar to the 5 April launches, the inversion during 7 April did not reach a state of equilibrium at the surface as seen in the 24 February launches, but instead continued to cool until the surface longwave radiation loss ceased after sunrise (Fig. 7). Similar to 5 April, a cooling process above the surface occurs between the 5:00 and 7:00 AST launches. In this case, the surface also has cooled a few degrees during the time frame, unlike the previously described case on 5 April.

3.4. 1 May 2009 case summary

A characteristic of the 1 May launches was the striking consistency and rapid rates of cooling between the surface and 800 m AGL over almost the entire period of record (Fig. 8), rather than recording cooling at the surface first then propagating upwards with height. This is most likely due to an important warming which occurred during the day from near-summertime shortwave radiation. On 1 May there

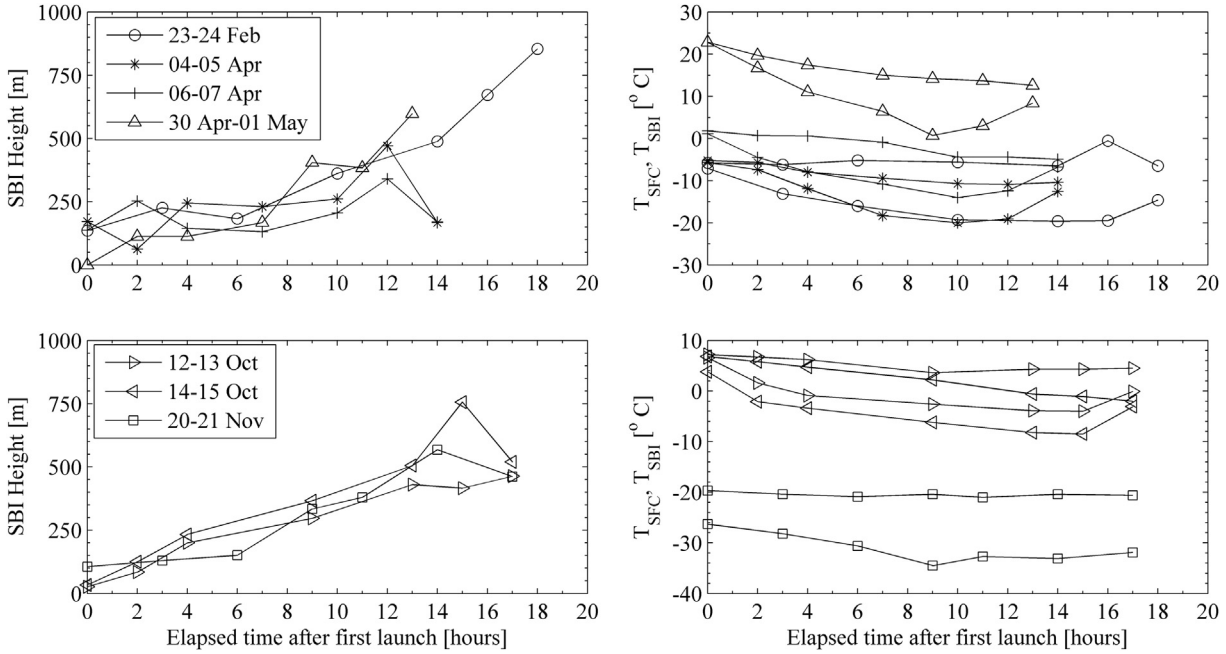

Fig. 6. On left: SBI height vs time (AST); On right: SBI top temperature (top line per color) vs time (AST) and surface temperature (bottom line per color) vs time (AST).

was a maximum of 750 Wm^{-2} of incoming radiation midday which resulted in significant surface warming, consequently increasing the upwelling longwave radiation that follows after sunset.

The set up and erosion of the SBI during the case study of 1 May is represented by a strong diurnal cycle that cannot be compared with the rest of the cases due to summertime incoming solar radiation and a very

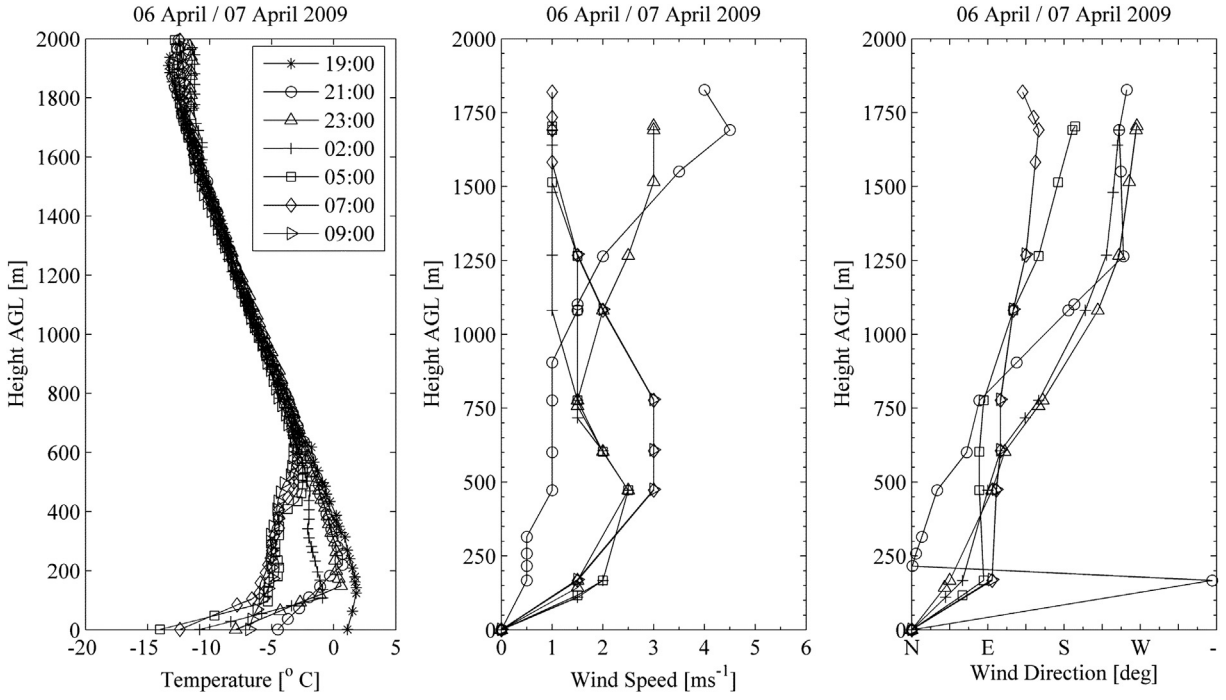

Fig. 7. Vertical structure of the SBI development post-sunset on April 7, 2009. Sunset – 20:01 AST.

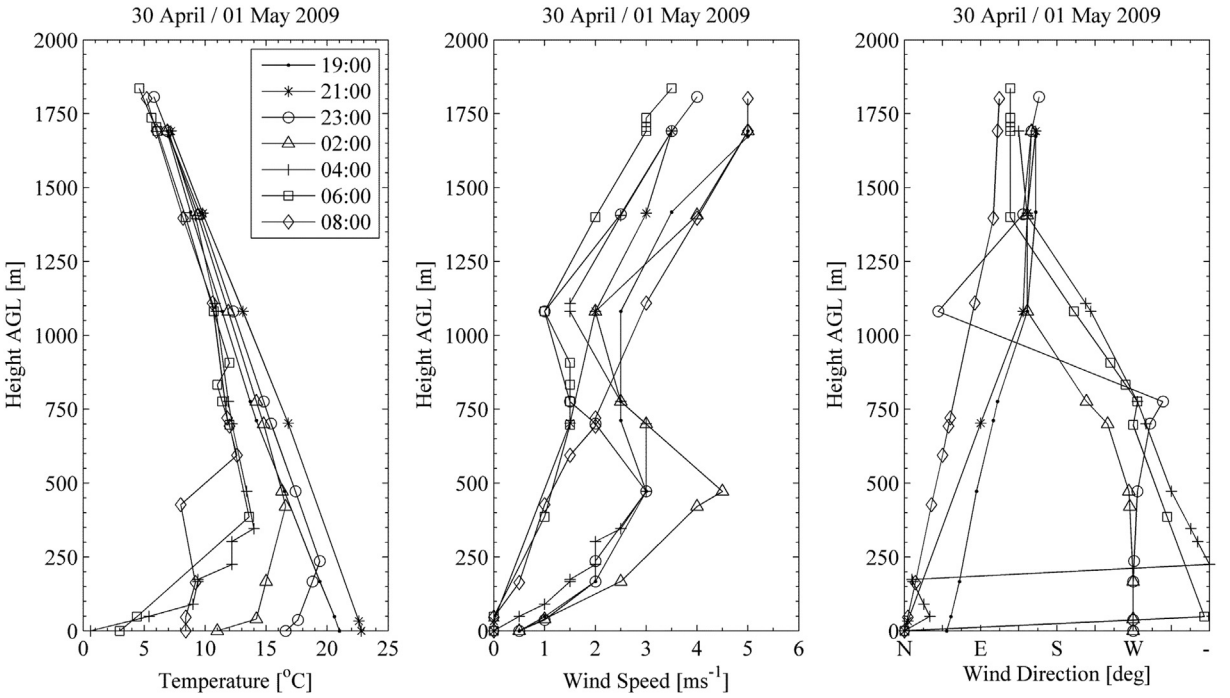

Fig. 8. Vertical structure of the SBI development post-sunset on May 1, 2009. Sunset – 21:19 AST.

long length of day. These launches do not exhibit the surface temperature reaching a minimum during the night and remaining the same as the inversion deepens in height as seen in previous launch dates. The temperature profiles in the free troposphere above the top height of the inversion layer for the 04:00, 06:00, and 08:00 AST launches are very similar. In the 08:00 AST launch it should be noted that, as the incoming radiation warms the surface, a very noticeable elevated inversion still exists even though the surface inversion has deteriorated.

3.5. 13 October 2009 case summary

This case shows a similar pattern to the April 7th case study, where the temperature decreases rapidly right after sunset (17:38 AST), and once the air mass in the inversion layer cools close to the minimum, the top height of the inversion layer begins to become higher in the atmosphere as the longwave upwelling radiation cooling proceeds in time. This deepening is weak for this case study (Fig. 9) compared to earlier case studies. It is important, to note that there is a different temporal interval between these launches (a 5 h gap between the 21:00 and 02:00 AST launches), and unlike the mainly 2 h time gap between launches, which indicates slower temporal atmospheric cooling.

3.6. 15 October 2009 case summary

This case shows a different profile than the one presented previously (13 October). It exhibits a much larger surface temperature fluctuation between daily highs and lows (Fig. 10). This is likely due to having three consecutive days of clear skies and calm weather conditions – maximizing incoming solar radiation each day which promotes surface warming during the daytime period. The surface warming during the daytime period introduces an important amount of energy stored at the surface which would have to be released after sunset to try to reach equilibrium with the cooler parts of the adjacent vertical atmosphere column. The wind profiles for 15 October 2009 indicate the presence of advection, with a wind maximum around 1200 m AGL during the 19:00 AST, 21:00 AST, and 02:00 AST launches. The levels at which these wind maxima occurred are coincident with the levels at which the temperature profile decreased less rapidly during the night (i.e. at about 50 m AGL from 02:00 to 06:00 AST), further strengthening the hypothesis that winds inhibit the cooling of the atmospheric profile post-sunset due to turbulent mixing.

3.7. 21 November 2009 case summary

Advective processes may be playing a role in this case, given the strength of the winds near 600 and

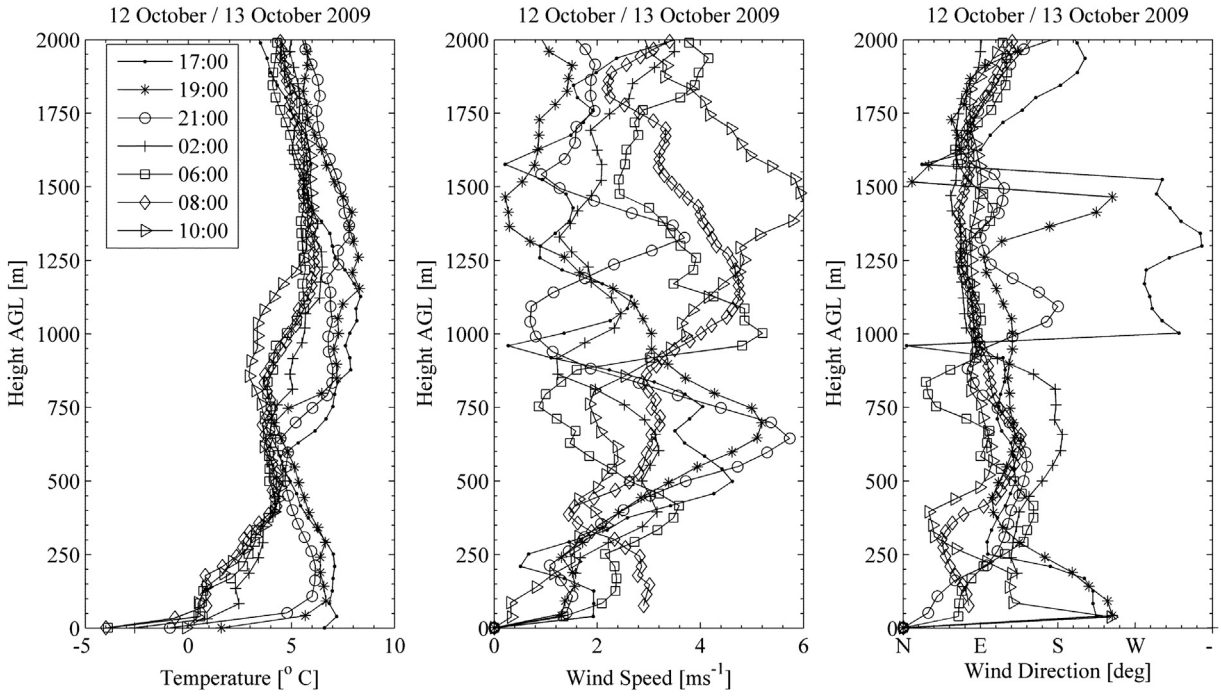

Fig. 9. Vertical structure of the SBI development post-sunset on October 13, 2009. Sunset – 17:38 AST Sunrise – at 07:36 AST.

1200 m AGL (Fig. 11). Even though these winds are high above the surface for the scale of this study, vertical transport or warm advection above the inversion could play a role in affecting the inversion. It appears the surface temperature decreases after sunset with a similar structure to the 1 May launches, but the atmospheric structure above the inversion remains isothermal likely due to the enhanced wind above

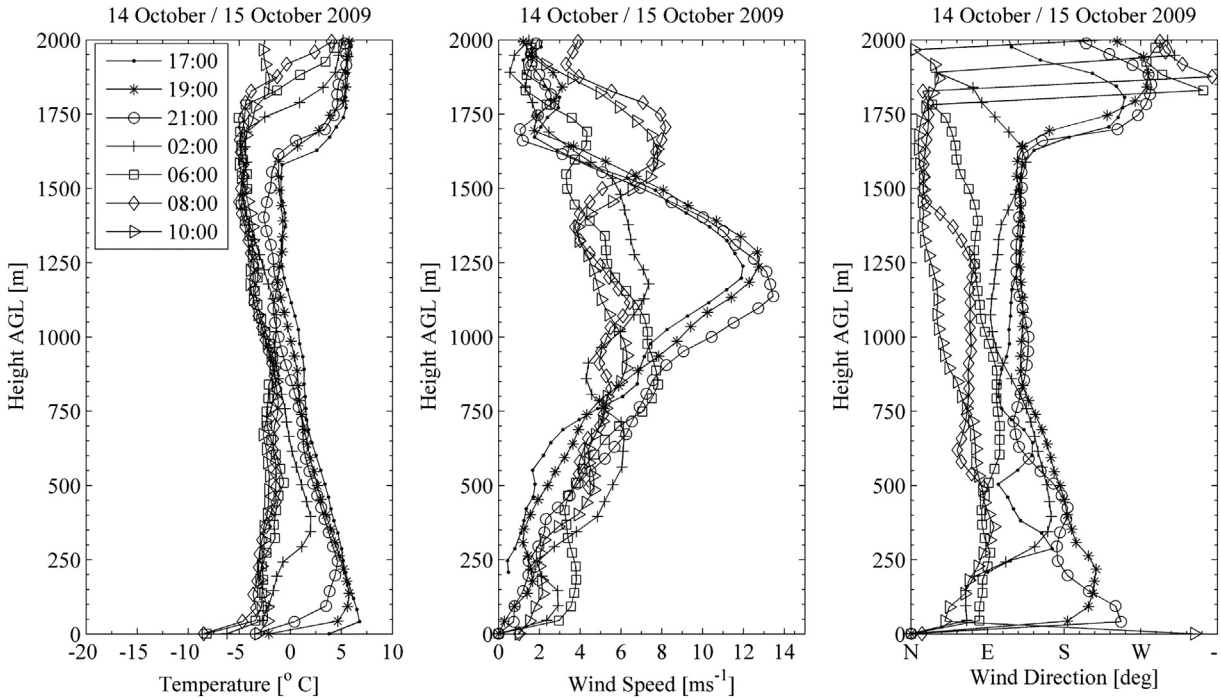

Fig. 10. Vertical structure of the SBI development post-sunset on October 15, 2009. Sunset – 17:27 AST. Sunrise – 07:45 AST.

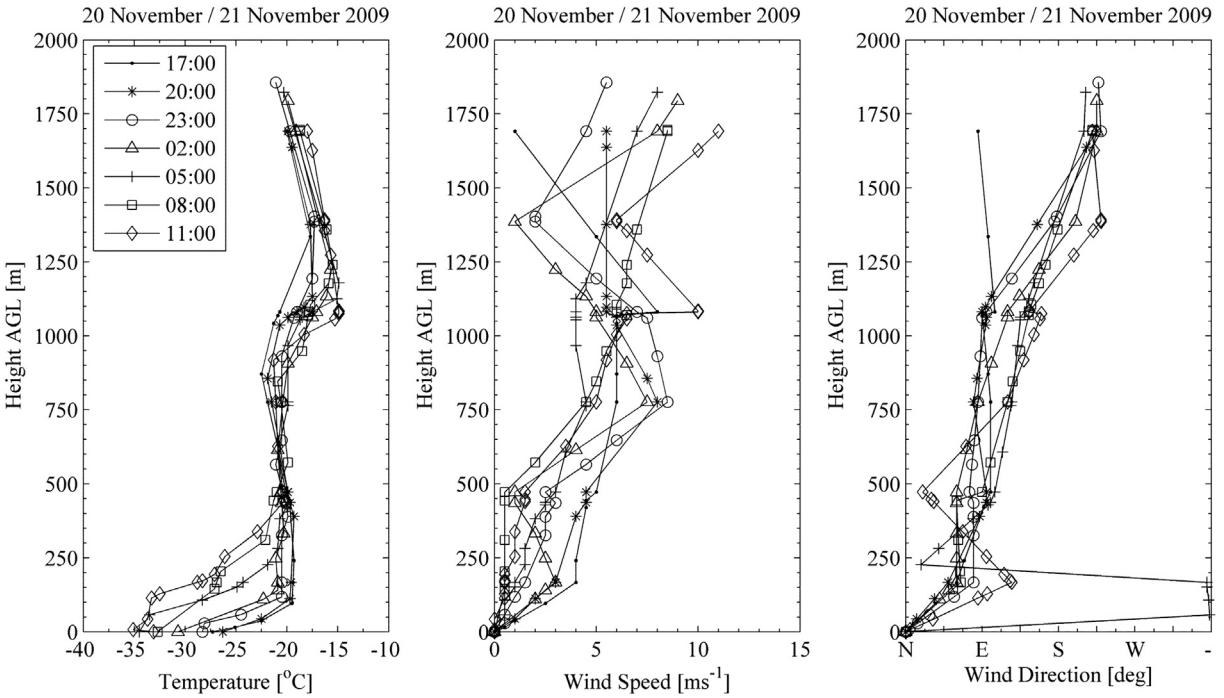

Fig. 11. Vertical structure of the SBI development post-sunset on November 21, 2009. Sunset – 15:28 AST. Sunrise – 09:48 AST.

150 m through the night. This final case study is unique of the others because daytime incoming shortwave radiation magnitudes are so low in November in interior Alaska.

4. Discussion and conclusions

4.1. Formation of SBI and the stratified layer

Here we consider the following variables: surface temperature, SBI top inversion height, vertical gradient of temperature and depth of the first stratified layer (Table 2). Each radiosonde was considered after the SBI was formed, or in other words at the first radiosonde where it was present. The first stratified layer that forms close to the surface will be the one responding to the changes in the cooling rate of the surface. This layer will acquire a certain depth. If the inversion layer does not have multiple microscale layers (multiple inversion layers with a neutral lapse rate in-between), then the depth of the SBI is the depth of the stratified layer close to the ground. However, in the process of forming the SBI and as the cooling proceeds in time, the formation of stratified layers as product of the surface cooling can be verified. Later, when the SBI tries to grow it will need to spend energy incorporating adiabatic layers, immediately above, into diabatic. This means that mixing in the stratified conditions needs to occur. In other words, to grow, the SBI "grabs the air mass from upper levels and put them downward into the stratified zone". This process is reflected by the existence of a neutral layer separating – often times by more than 100 m thickness – the stratified layer below from the adiabatic cold layer above. Table 2 illustrates the evolution of the main parameters after the SBI was formed, based on the surface temperature, the top height of the SBI, the surface layer stratification [dT/dZ], and the depth of the stratified layer.

The results gathered during these 42 individual radiosonde launches for seven case studies present a suite of information about the structure, evolution, and thermodynamics of the SBI formation and breakup during transitions in the ABL diurnal cycle at high latitudes. Although each case study presents a unique record due to variability introduced by the incoming solar radiation and snow cover, several generalizations emerged which provide new insights into the formation of the SBI in terms of these variables. Overall, for each of the seven case studies, the minimum surface temperature is reached at sunrise, or just before sunrise, as depicted in Table 2. During 5 of 7 case studies, the surface temperature drops the fastest within the first hours after sunset (−3 °C/hr to −6 °C/hr). The

Table 2
SBI top height, surface temperature evolution and surface layer stratification. First column indicate the radiosonde data, second column is the launching time in UTC, third column is the surface temperature in [°C], fourth column is the height of the SBI in [m] AGL, the fifth column is the surface layer stratification in [°C/100 m] and the sixth column is the depth of the stratified layer [m] when the SBI is stratified.

Launch	Time	T_{SFC} [°C]	H_{SBI} [m]	dT/dZ [°C/100 m]	Hstr (m)
23-Feb-09	16	−7.1	136	0.95	N/A
23-Feb-09	19	−13.1	226	3.05	N/A
23-Feb-09	22	−16	183	5.9	N/A
24-Feb-09	2	−19.3	362	3.78	73
24-Feb-09	6	−19.6	488	2.68	237
24-Feb-09	8	−19.5	672	2.82	516
24-Feb-09	10	−14.6	854	0.94	735
4-Apr-09	19	−5.7	172	0.29	120
4-Apr-09	21	−7.4	63	2.7	N/A
4-Apr-09	23	−11.9	245	1.6	107
5-Apr-09	2	−18.3	231	3.85	35
5-Apr-09	5	−20	261	3.56	115
5-Apr-09	7	−19.1	471	1.74	N/A
5-Apr-09	9	−12.6	167	1.31	63
6-Apr-09	19	1.1	138	0.5	123[a]
6-Apr-09	21	−4.5	253	2.1	219[a]
6-Apr-09	23	−7.9	145	5.9	N/A
7-Apr-09	2	−10.8	132	7.5	N/A
7-Apr-09	5	−14	206	4.7	94
7-Apr-09	7	−12.4	340	2.4	123
7-Apr-09	9	−6.8	170	1.1	173
30-Apr-09	19	22.8	–	–	N/A
30-Apr-09	21	16.7	113	2.7	N/A
30-Apr-09	23	11	113	5.7	138
1-May-09	2	6.4	168	5.1	95
1-May-09	4	0.7	405	3.3	N/A
1-May-09	6	3	384	2.8	73
1-May-09	8	8.4	598	0.7	N/A
12-Oct-09	17	6.6	26.3	2.3	N/A
12-Oct-09	19	1.6	84	6.1	N/A
12-Oct-09	21	−0.9	200	3.6	67.9
13-Oct-09	2	−2.6	297	2.1	87
13-Oct-09	6	−3.9	430	1.9	47.6
13-Oct-09	8	−4	416	2	70
13-Oct-09	10	−0.1	463	1	19
14-Oct-09	17	3.8	33.4	9	N/A
14-Oct-09	19	−2.1	125	6.3	76.7
14-Oct-09	21	−3.4	233	3.5	113
15-Oct-09	2	−6.2	366	2.3	198
15-Oct-09	6	−8.2	505	1.5	87
15-Oct-09	8	−8.5	756.4	1	72
15-Oct-09	10	−3.1	520	0.2	66
20-Nov-09	17	−26.3	105.7	6.3	108
20-Nov-09	20	−28.2	130	6	133
20-Nov-09	23	−30.6	151	6.4	143
21-Nov-09	2	−34.5	334	4.2	332
21-Nov-09	5	−32.7	380	3.1	382
21-Nov-09	8	−33.1	568	2.2	450
21-Nov-09	11	−31.9	462	2.5	465

[a] Denotes the stratified layer is capped of a thin isothermal layer.

temperature column begins to cool upwards after this initial cooling pulse at the surface. An exception to this result is represented by the two cases on 1 May and 21 November, which did not have the most significant surface temperature drop at the beginning of the night immediately after sunset. The case of 1 May initiates after extreme daytime heating at the beginning of the case study, and 21 November is a time of year when there is very little solar radiation to warm up the surface during the short day, therefore the sun setting did not introduce major contrasting factors in terms of temperature changes. However it can be concluded that the minimum surface temperature was reached in a time lapse ranging between 7 and 14 h after sunset, with an average of 10.6 h after sunset (Table 1). Fig. 6 displays the deepening of the inversion with time through the night until sun rises the next morning. According to this data, all of the launches show a similar pattern in that the temperature of the top of the SBI remained near isothermal on the top as the inversion deepened with height through the night.

When the rate of cooling provided by the high resolution temperature profiling is analyzed, it appears on two launches (24 February and 13 October) that the surface cooling is interrupted, indicating that in the condition of the experiments, a radiative equilibrium has been reached giving the origin to a minimum surface temperature during the diurnal cycle between 2:00 and 8:00 AST (Fig. 6).

The April 7th case result shows the influence of short-lived changes in near surface winds on propagating a surface cold pulse upward into the atmosphere and this result could not be empirically obvious by analyzing the vertical profile under the standard temporal resolution of 03:00 and 15:00 AST weather balloon launches.

4.2. Sodar profiling of the SBI: comparison to radiosondes

Continuous SODAR profiling allows the vertical structure of the ABL to be examined in great detail at 20 m resolution, within the limits of the maximum height the instrument can reach during the extreme condition in interior of Alaska. One case was selected on 15 October where radiosonde and SODAR profiles are coincident. Fig. 12 displays the acoustic sounding profiles integrated over 3 h previous to the radiosonde launches at 21:00, 2:00, 6:00, 8:00 and 10:00 AST on 15 October. Table 3 illustrates the comparison between the height of the SBI retrieved by SODAR and that of the closest radiosonde after applying the methodology

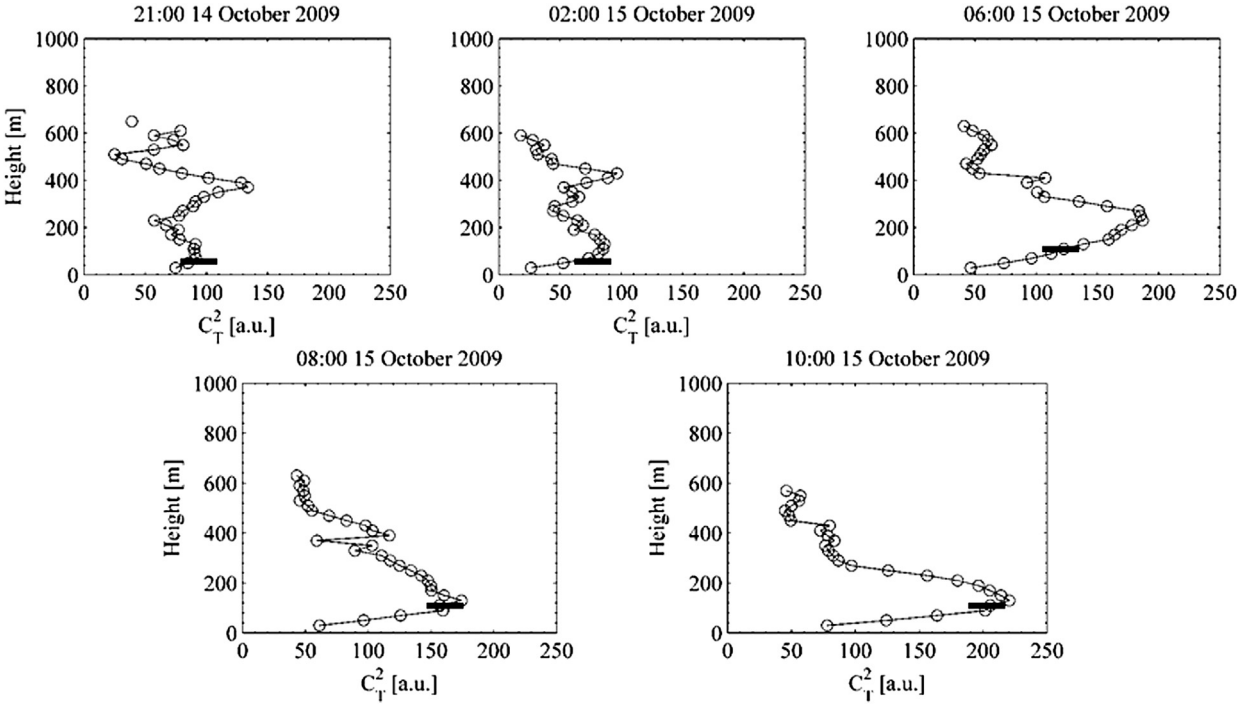

Fig. 12. Sodar vertical profiles of the coefficient of thermal turbulence structure C_T^2. The vertical resolution is 20 m and the temporal resolution 15 min. Each profile results in a 3 h accumulation of acoustic soundings. Top panel left represent the series of profiles from 12:00 AST of 14 October to 15:00 AST 15 October. Top central panel correspond to the period of time from 15:00 AST 15 October to 18:00 AST 15 October. Top right panel represents the period of time form 18:00 AST 15 October to 21:00 AST 15 October. Low panel left is the 00:00 AST 15 October to 03:00 AST 15 October and low panel right corresponds to the period from 03:00 AST 15 October to 06:00 AST 15 October.

described previously. It was found that the SBI height based on both the SODAR instrumentation and radiosondes were within 50 m of one another. Table 3 indicates convergence of both instruments in indicating the height of the SBI with the exception of the profile representing 21:00 AST due to the poor signal to noise ratio. It is clear that the high resolution of SODAR profiling allow determination of the fine thermal structure of the ABL. This is seen in the slope changes of the thermal turbulence profile C_T^2 indicative of the presence of stratified layers.

Table 3
Comparison table between height of the SBI determined by radiosonde system and sodar profiling. First column indicate the radiosonde launch time in UTC time. Second column is the height of the SBI retrieved by the radiosonde. Third column is the retrieved height by sodar.

14–15 October 2009	H_{RAOBS} [m]	H_{Sodar} [m]
21:00	233	230
02:00	366	370
06:00	505	470
08:00	756	530[a]
10:00	520	490

[a] Out of range for the sodar profiler.

4.3. Conclusions

This dataset represents a detailed examination of the temporal evolution of the SBI driven by radiational cooling at a sub-arctic location during the spring and autumn seasons. Several important observations resulted from this study.

The growing of the SBI (i.e. thickening vertically) was found to occur only after the surface temperature converges to a minimum temperature. This means that during the ABL transition two cooling regimes have been identified: one is a transient cooling to reach the surface temperature minimum and the second is a steady state columnar cooling in which the boundary condition at the surface somehow remains in equilibrium as a result of moving the upper boundary thickening the air mass within the SBI searching for the equilibrium point between radiation exchange and momentum. These conditions will act in opposite ways. If winds develop overnight the SBI will be erased and completely mixed down.

When snow cover is present, the vertical cooling will happen more rapidly because of high surface albedo and the inability of the ground to absorb significant amounts of radiation during the day.

The presence of short-lived wind pulses can serve to modify the evolution of the vertical temperature profile by slowing down heat loss from outgoing radiation through horizontal mixing or, in other words, "thermalizing" the ABL.

For example, on 24 February, the 19:00 AST launch indicates a warming of the atmosphere above the inversion, which corresponds well with a wind increase on the wind profile. Without this wind increase, the data suggests that we would see a cooling of the profile in this layer of the atmosphere. Although difficult to discern in comparison with other launches on the same date due to a poor vertical resolution of winds, this effect is apparent when looking at inversion data where there is much better vertical resolution in wind data (autumn launches) due to a change in instrumentation. In a case with higher resolution data, such as the 15 October case, higher winds (4 m/s) around 50 m AGL suggested a reduction in the cooling rate, which is not necessarily reflected in the surface temperature, but slightly above the surface at 50 m AGL.

These results bear directly on considerations of climate change impacts on local climates. If the weather of interior Alaska becomes warmer and more dynamic, temperature inversions may not be as common or as steep, as identified in current trends in a Fairbanks inversion climatology study by Bourne et al. (2010). From the observational results presented here, the mechanisms by which climate change may alter inversion characteristics would come from increasing downwelling longwave radiation due to increasing cloudiness and increasing winds.

Acknowledgments

The authors wish to thank Don Morton (UAF/Arctic Region Supercomputing Center), Eugene Petrescu (NWS/Anchorage), and Nicole Mölders (UAF/Atmospheric Sciences) for fruitful discussions. Funding contributions to this project came from NOAA grant NA06OAR4600179 "Social Vulnerability of Alaska Communities to Climate Change". Funding was also supported in part by a UAF Center for Global Change Student Research Grant with funds from the International Arctic Research Center (NSF ARC-0652838), as well as from NOAA's Student Career Employment Program. Additional support came from the National Weather Service's COMET program and JAMSTEC (through its cooperative agreement with IARC). WiBLEx was supported by Fairbanks North Star Borough Air and the Department of Environmental Conservation of Alaska. The authors thank the comments from the two anonymous reviewers.

References

André, J.C., Mahrt, L., 1981. The nocturnal surface inversion and influence of clear-air radiative cooling. J. Atmos. Sci. 39, 864–878.

Beyrich, F., Weill, A., 1993. Some aspects of determining the stable boundary layer depth from SODAR data. Bound.-Layer Meteorol. 63, 97–116.

Bourne, S.M., Bhatt, U.S., Zhang, J., Thoman, R., 2010. Surface-based temperature inversions in Alaska from a climate perspective. Atmos. Res. 95, 353–366.

Bradley, R.S., Keimeg, F.T., Diaz, H.F., 1992. Climatology of surface-based inversions in the North American Arctic. J. Geophys. Res. 97, 15699–15712.

Brown, E.H., Hall Jr., F.F., 1978. Advances in atmospheric acoustics. Rev. Geophys. Space Phys. 16, 47–110.

Cermak, J.E., 1971. Laboratory simulation of the atmospheric boundary layer. AIAA J. 9 (9), 1746–1754.

Coulter, R.L., Kallistratova, M.A., 2004. Two decades of progress in SODAR techniques: a review of 11 ISARS proceedings. Meteorol. Atmos. Phys. 85, 3–19.

Estournel, C., Guedalia, D., 1985. Influence of geostrophic wind on atmospheric nocturnal cooking. J. Atmos. Sci. 42 (23), 2695–2698.

Hartmann, B., Wendler, G., 2005. Climatology of the Winter surface temperature inversion in Fairbanks, Alaska. In: 85th AMS Annual Meeting, San Diego, CA, p. 187.

Hogan, A., Ferrick, M., 1997. Winter morning air temperature. J. Appl. Meteorol. 36, 52–69.

Holmgren, B., Spears, L., Wilson, C., Benson, C.S., 1975. Acoustic soundings of the Fairbanks temperature inversions. In: Weller, G., Bowling, S.A. (Eds.), Climate of the Arctic: Proceedings of the AAAS-AMS Conference, Fairbanks, Alaska, 1973. University of Alaska Geophysical Institute, pp. 293–306.

Kahl, J.D., 1990. Characteristics of the low-level temperature inversion along the Alaskan Arctic coast. Int. J. Climatol. 10, 537–548.

Kahl, J.D., Serreze, M.C., Schnell, R.C., 1992. Tropospheric low-level temperature inversions in the Canadian arctic. Atmos-Ocean 30 (4), 511–529.

Mayfield, J.A., Fochesatto, G.J., 2013. The layered structure of the winter atmospheric boundary layer in the Interior of Alaska. J. Appl. Meteorol. Climatol. 52, 953–973.

Molders, N., Kramm, G., 2010. A case study on wintertime inversions in interior Alaska with WRF. Atmos. Res.. http://dx.doi.org/10.1016/j.atmosres.2009.06.002.

Morton, D., 2009. Comparison of ARSCwrf surface variables with observations. In: The Alaska Weather Symposium, Fairbanks, AK, 10–12 March 2009.

Neff, W.D., 1975. Quantitative Evaluation of Acoustic Echoes from the Planetary Boundary Layer, p. 34. National Oceanic and Atmospheric Administration Tech. Rep. ERL 322-WPL 38.

Neff, W.D., Coulter, R.L., 1988. Acoustic remote sensing. In: Lenschow, D.H. (Ed.), Probing the Atmospheric Boundary Layer, Amer. Meteor. Soc., pp. 201–235.

Pepin, N.C., Schaefer, M.K., Riddy, L.D., 2009. Quantification of the cold air pool in Kevo Valley, Finnish Lapland. Weather 64 (3), 60–67.

Seidel, D.J., Ao, C.O., Li, K., 2010. Estimating climatological planetary boundary layer heights from radiosonde observations: comparison of methods and uncertainty analysis. J. Geophys. Res. 115, D16113. http://dx.doi.org/10.1029/2009JD013680.

Serreze, M.C., Kahl, J.D., Schnell, R.C., 1992. Low-level temperature inversions of the Eurasian Arctic and comparisons with Soviet drifting stations. J. Clim. 5, 615−630.

Stevens, E., 2009. An investigation of the relationship between surface temperatures and the establishment of snowpack during October in Fairbanks, Alaska. Atmos. Res. 95 (2−3), 307−313.

Stull, R.B., 1988. An Introduction to Boundary Layer Meteorology. Kluwer, p. 666.

Tilley, J.S., Weatherby, C., 2001. On the sensitivity of simulated subarctic wintertime inversions to PBL parameterization. In: Preprints, 11th PSU/NCAR Mesoscale Model Users' Workshop, 25−27 June, Boulder, CO, pp. 106−109.

Walsh, J.E., Jasperson, W.H., Ross, B., 1985. Influences of snow cover and soil moisture on monthly air temperature. Mon. Weather Rev. 113, 756−768.

Wendler, G., Jayaweera, K.O.L.F., 1972. Some measurements on the development of the surface inversion in Central Alaska during winter. Pure Appl. Geophys. 92, 209−221.

Wendler, G., Nicpon, P., 1974. Low-level temperature inversions in Fairbanks, Central Alaska. Mon. Weather Rev. 103, 34−44.

Wexler, H., 1936. Cooling in the lower atmosphere and the structure of Polar continental air. Mon. Weather Rev. 64 (4), 122−136.